JOC Article

Molecular Triads Composed of Ferrocene, C_{60}, and Nitroaromatic Entities: Electrochemical, Computational, and Photochemical Investigations

Melvin E. Zandler,[†] Phillip M. Smith,[†] Mamoru Fujitsuka,[‡] Osamu Ito,*[,‡] and Francis D'Souza*[,†]

Department of Chemistry, Wichita State University, 1845 Fairmount, Wichita, Kansas 67260-0051, and Institute of Multidisciplinary Research for Advanced Materials, Chemical Reaction Science, Tohoku University, Katahira, Sendai, 980-8577, Japan

Francis.DSouza@wichita.edu

Received June 18, 2002

Synthesis and physicochemical characterization of a series of molecular triads composed of ferrocene, C_{60}, and nitroaromatic entities are reported. Electrochemical studies revealed multiple redox processes involving all three redox active ferrocene, C_{60}, and nitrobenzene entities. Up to eight redox couples within the accessible potential window of *o*-dichlorobenzene containing 0.1 M (TBA)-ClO_4 are observed. A comparison between the measured redox potentials with those of the starting compounds revealed absence of any significant electronic interactions between the different redox entities. The geometric and electronic structure of the triads are elucidated by using ab initio B3LYP/3-21G(*) methods. In the energy-optimized structures, as predicted by electrochemical studies, the first HOMO orbitals are found to be located on the ferrocene entity, while the first LUMO orbitals are mainly on the C_{60} entity. The coefficients of the subsequent LUMO orbitals track the observed site of electrochemical reductions of the triads. The photochemical events of the triads are probed by both steady-state and time-resolved techniques. The steady-state emission intensities of the triads and the starting dyad, 2-(ferrocenyl)fulleropyrrolidine, are found to be completely quenched compared to fulleropyrrolidine bearing no redox active substituents. The subpicosecond and nanosecond transient absorption spectral studies revealed efficient charge separation (and rapid charge recombination) in the triads, and this has been attributed to the close spacing of the redox entities of the triad to one another.

Introduction

Studies on fullerenes linked to multiple redox- and/or photoactive molecular entities[1−5] have seen a rapid growth since they are potential candidates for constructing molecular/supramolecular electronic devices[6−11] and artificial light energy-harvesting systems.[12−26] Toward this, a variety of electron donors such as porphyrin, ferrocene, *N*,*N*-dimethylaminophenyl, ruthenium(II) tris-bipyridyl, and tetrathiafulvarene have been employed to form fullerene-electron donor-type dyads while a few electron acceptors such as benzoquinone derivatives, spiroannelated methano groups, cyano groups, fluorine

* To whom correspondence should be addressed. Fax: +(316) 978-3431.
† Wichita State University.
‡ Tohoku University.

(1) Martin, N.; Sachez, B.; Illescas, B.; Perez, I. *Chem. Rev.* **1998**, *98*, 2427−2547.
(2) Prato, M.; Maggini, M. *Acc. Chem. Res.* **1998**, *31*, 519−526.
(3) Carano, M.; Ceroni, P.; Paolucci, F.; Roffia, S.; Da Ros, T.; Prato, M.; Sluch, M. I.; Pearson, C.; Petty, M. C.; Bryce, M. R. *J. Mater. Chem.* **2000**, *10*, 269−273.
(4) *Fullerene and Related Structures*; Hirsch, A., Ed.; Springer: Berlin, 1999; Vol. 199.
(5) Long, N. J. *Angew. Chem., Int. Ed. Engl.* **1995**, *34*, 21−38.
(6) *Molecular Electronic-Science and Technologie*; Aviram, A., Ed.; Engineering Foundation: New York, 1989.
(7) Aviram, A.; Ratner, M. *Chem. Phys. Lett.* **1974**, *29*, 277−283.
(8) *Electronic Materials and Devices*; Ferry, D. K.; Bird, J. P., Eds.; Academic: San Diego, CA, 2001.
(9) *Introduction to Molecular Electronics*; Petty, M. C.; Bryce, M. R.; Bloor, D., Eds.; Oxford University Press: New York, 1995.
(10) Prasad, P. N.; Williams, D. J. *Introduction to Nonlinear Optical Effects in Molecules and Polymers*; Wiley: New York, 1991.
(11) Nalwa, H. S. *Adv. Mater.* **1993**, *5*, 341−358.
(12) *Photoinduced Electron Transfer*; Fox, M. A., Channon, M., Eds.; Elsevier: Amsterdam, 1988; Parts A−D.
(13) Kurreck, H.; Huber, M. *Angew. Chem., Int. Ed. Engl.* **1995**, *34*, 849−866.
(14) Staab, H. A.; Feurer, A.; Hauck, R. *Angew. Chem., Int. Ed. Engl.* **1994**, *33*, 2428−2431.
(15) Roest, M. R.; Verhoeven, J. W.; Schiddeboon, W.; Warman, J. M.; Lawson, J. M.; Paddon-Row: M. N. *J. Am. Chem. Socc.* **1996**, *118*, 1762−1768.
(16) Maruyama, K.; Osuka, A. *Pure Appl. Chem.* **1990**, *62*, 1511−1520.
(17) Gust, D.; Moore, T. A. *Science* **1989**, *244*, 35−41.
(18) (a) Gust, D.; Moore, T. A. *Top. Curr. Chem.* **1991**, *159*, 103−151. (b) Gust, D.; Moore, T. A.; Moore, A. L. *Pure Appl. Chem.* **1998**, *70*, 2189−2200.
(19) Gust, D.; Moore, T. A.; Moore, A. L. *Acc. Chem. Res.* **1993**, *26*, 198−205.
(20) Wasielewski, M. R. *Chem. Rev.* **1992**, *92*, 435−461.
(21) Paddon-Row, M. N. *Acc. Chem. Res.* **1994**, *27*, 18−25.
(22) Sutin, N. *Acc. Chem. Res.* **1983**, *15*, 275−284.
(23) Bard, A. J.; Fox, M. A. *Acc. Chem. Res.* **1995**, *28*, 141−145.
(24) Meyer, T. J. *Acc. Chem. Res.* **1989**, *22*, 163−170.
(25) Piotrowiak, P. *Chem. Soc. Rev.* **1999**, *28*, 143−150.
(26) Imahori, H.; Sakata, Y. *Adv. Mater.* **1997**, *9*, 537−546.

10.1021/jo020417i CCC: $22.00
Published on Web 11/06/2002

SCHEME 1

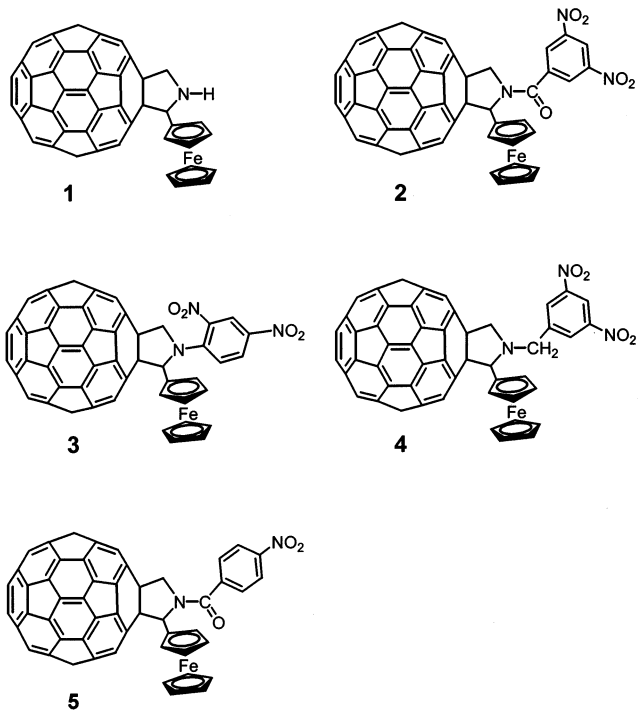

atoms, TCNQ and DCNQI derivatives, ammonium cations, and nitroaromatic substituents have been employed to form covalently linked fullerene-electron acceptor-type dyads.[1−5,26−28] In addition, a few elegantly designed triads and tetrads bearing one or more different electron donor and/or acceptor entities have been synthesized, and studied.[15,26−31]

Recently, we reported on the synthesis and physicochemical characterization of a ferrocene−C_{60}−dinitrobenzene triad, that is, a donor−(acceptor-1)−(acceptor-2)-type triad[32] (compound **2** in Scheme 1). Efficient intramolecular photoinduced charge separation and charge recombination processes were observed in this triad. Here, we have extended this study by involving three additional triads bearing ferrocene, C_{60}, and nitroaromatic entities. This study has been particularly undertaken to verify the ab initio B3LPY/3-21G(*) computational approach reported earlier to track the sequence (site) of electron transfer involving all three redox active groups. The geometric and electronic structures, as well as the sequence of the site of electron transfer in the newly synthesized triads, have been elucidated from optical absorption, electrochemical, and ab initio B3LPY/3-21G(*) methods. Using steady-state and time-resolved emission techniques, we have also probed the excited-state photoinduced electron-transfer processes for the investigated triads.

Experimental Section

Chemicals. Buckminsterfullerene, C_{60} (+99.95%), was either from BuckyUSA (Bellaire, TX) or SES Research (Houston, TX). *o*-Dichlorobenzene for electrochemical studies was dried over CaH_2 and distilled under vacuum prior to the experiments. The (TBA)ClO_4 was recrystallized from ethanol and dried in a vacuum oven at 35 °C for 10 days. The synthesis and characterization of 2-(ferrocenyl)fulleropyrrolidine, **1**, and *N*-(3′,5′-dinitrobenzoyl)-2-(ferrocenyl)-fulleropyrrolidine, **2**, are given elsewhere.[32] *J* values are given in hertz.

***N*-(2′,4′-Dinitrophenyl)-2-(ferrocenyl)fulleropyrrolidine**, **3.** This was prepared by using Sanger's method reported earlier for the synthesis of *N*-(2′,4′-dinitrophenyl)-2-(phenyl)-fulleropyrrolidine.[33a] To a solution of 2-(ferrocenyl)-fulleropyrrolidine (20 mg) dissolved in dry THF (25 mL) was added NaH (2 mg) and the mixture was stirred until hydrogen evolution ceased. Then, 1-fluoro-2,4-dinitrobenzene (15 μL) was added, and the solution was stirred for another 6 h. At the end, water (1 mL) was added, and the solution was evaporated under reduced pressure. The compound was purified over silica gel column using toluene as an eluent: yield 55%; ^{1}H NMR in $CDCl_3/CS_2$ (1:1 v/v), δ ppm, 9.06 (s, 1H, dinitrophenyl H), 8.42 (m, 1H, dinitrophenyl H), 7.30 (m, 1H, dinitrophenyl H), 5.53 (s, 1H, pyrrolidine H), 5.00, 4.89 (d, d, 2H, J = 6, J = 6, pyrrolidine H), 4.52, 4.46, 4.08, 4.19 (s, s, s, s, 1H, 1H, 1H, 1H, ferrocene H), 4.32 (s, 5H, ferrocene H); UV−visible in *o*-dichlorobenzene, λ_{max} nm, 382 (sh), 432; ESI mass in CH_2Cl_2 calcd 1113.8, found 1114.2.

***N*-(3′,5′-Dinitrobenzyl)-2-(ferrocenyl)fulleropyrrolidine**, **4.** To a suspension of 2-(ferrocenyl)fulleropyrrolidine (30 mg) in dry CH_2Cl_2 (40 mL) containing triethylamine (1.1 equiv) was added 3,5-dinitrobenzyl chloride (21 mg) and the mixture was refluxed for 5 h. The compound was purified over a silica gel column using toluene/ethyl acetate (97:3 v/v) as an eluent: yield 27%; ^{1}H NMR in $CDCl_3/CS_2$ (1:1 v/v), δ ppm, 8.93 (s, 1H, dinitrobenzyl H), 8.51 (s, 2H, dinitrobenzyl H), 5.53 (s, 1H, pyrrolidine H), 5.26 (s, 2H, methylene H), 4.99, 4.85 (d, d, 2H, *J6*, *J6*, pyrrolidine H), 4.51, 4.43, 4.16 (s, s, s, 1H, 1H, 2H, ferrocene H), 4.32 (s, 5H, ferrocene H); UV−visible in *o*-dichlorobenzene, λ_{max} nm, 330 (sh), 432; ESI mass in CH_2Cl_2 calcd; 1127.8, found 1129.1.

***N*-(4′-Mononitrobenzoyl)-2-(ferrocenyl)fulleropyrrolidine**, **5.** To a suspension of 2-(ferrocenyl)fulleropyrrolidine (20 mg) in dry CH_2Cl_2 (25 mL) containing triethylamine (1.1 equiv) was added excess of 4-nitrobenzoyl chloride, and the solution was stirred for 3 h. The compound was purified over a silica gel column using toluene/ethyl acetate (95:5 v/v) as an eluent: yield 34%; ^{1}H NMR in $CDCl_3/CS_2$ (1:1 v/v), δ ppm, 8.21 (m, 4H, mononitrobezoyl H), 5.54 (s, 1H, pyrrolidine H), 4.99, 4.87 (d, d, 2H, J = 7, J = 7, pyrrolidine H), 4.53, 4.46, 4.16 (s, s, s, 1H, 1H, 2H, ferrocene H), 4.32 (s, 5H, ferrocene H); UV−visible in *o*-dichlorobenzene, λ_{max} nm, 432, 316; ESI mass in CH_2Cl_2 calcd 1096.8, found 1096.3.

Instrumentation. UV−visible spectral measurements were carried out with a Shimadzu Model 1600 UV−visible spectrophotometer. The fluorescence was monitored by using a Spex Fluorolog spectrometer. A right angle detection method was

(27) Diederich, F.; Gomez-Lopez, M. *Chem. Soc. Rev*. **1999**, *28*, 263−277.
(28) Guldi, D. M. *Chem. Commun*. **2000**, 321−327.
(29) (a) Liddell, P. A.; Kuciauskas, D.; Sumida, J. P.; Nash, B.; Nguyen, D.; Moore, A. L.; Moore, T. A.; Gust, D. *J. Am. Chem. Socc.* **1997**, *119*, 1400−1405. (b) Kuciauskas, D.; Liddell, P. A.; Lin, S.; Johnson, T. E.; Wighorn, S. L.; Lindsey, J. S.; Moore, A. L.; Moore, T. A.; Gust, D. *J. Am. Chem. Soc.* **1999**, *121*, 8604−8614. (c) Carbonera, D.; Di Valentin, M.; Corvaja, C.; Agostini, G.; Giacometti, G.; Liddell, P. A.; Kuciauskas, D.; Moore, A. L.; Moore, T. A.; Gust, D. *J. Am. Chem. Soc.* **1998**, *120*, 4398−4405.
(30) Luo, C.; Guldi, D. M.; Imahori, H.; Tamaki, K.; Sakata, Y. *J. Am. Chem. Soc.* **2000**, *122*, 6535−6551.
(31) D'Souza, F.; Deviprasad, G. R.; El-Khouly, M. E.; Fujitsuka, M.; Ito, O. *J. Am. Chem. Soc.* **2001**, *123*, 5277−5284 and references therein.
(32) D'Souza, F.; Zandler, M. E.; Smith, P. M.; Deviprasad, G. R.; Arkady, K.; Fujitsuka, M.; Ito, O. *J. Phys. Chem. A* **2002**, *106*, 649−656.
(33) (a) Deviprasad, G. R.; Rahman, M. S.; D'Souza, F. *Chem. Commun*. **1999**, 849−850. (b) de la Cruz, P.; de la Hoz, A.; Langa, F.; Martin, N.; Perez, M. C.; Sanchez, L. *Eur. J. Org. Chem*. **1999**, 3433−3436. (c) Guldi, D. M.; Maggini, M.; Scorrano, G.; Prato, M. *J. Am. Chem. Soc.* **1997**, *119*, 974−980. (d) Herranz, M. A.; Illescas, B.; Nazario, M.; Luo, C.; Guldi, D. M. *J. Org. Chem*. **2000**, *65*, 5728−5738.

used. ^{1}H NMR studies were carried out on a Varian 400 MHz spectrometer. Tetramethylsilane (TMS) was used as an internal standard. Cyclic voltammograms were obtained by using a conventional three-electrode system on an EG&G model 263A potentiostat/galvanostat or a model AFCB1 bipotentiostat from Pine Instrument Co. (Grove City, PA). A platinum disk electrode was used as the working electrode. A platinum wire served as the counter electrode. An Ag/AgCl reference electrode, separated from the test solution by a fritted supporting electrolyte/solvent bridge, or Ag/Ag^+ pseudoreference electrodes were used. The potentials were referenced to an internal ferrocene/ferrocenium redox couple. All the solutions were purged prior to spectral and electrochemical measurements using argon gas.

Computational Calculations. The computational calculations were performed by using the *Gaussian 98*[34] software package. The graphics of the HOMO and LUMO molecular orbital coefficients were generated with the help of *GaussView* software. The compounds were fully optimized to a stationary point on the Born−Oppenheimer potential energy surface. The frontier HOMO and LUMOs were calculated on fully optimized structures.

Time-Resolved Absorption Measurements. Subpicosecond transient absorption spectra were recorded by the pump and probe method. Samples were excited with a second harmonic generation (SHG, 388 nm) of output from a femtosecond Ti:sapphire regenerative amplifier seeded by SHG of a Er-dropped fiber (Clark-MXRCPA-2001 plus, 1 kHz, fwhm 150 fs). The excitation light was depolarized. The monitor white light was generated by focusing the fundamental of the laser light on a flowing D_2O/H_2O cell. The transmitted monitor light was detected with a dual MOS linear image sensor (Hamamatsu Photonics, C6140) or InGaAs photodiode array (Hamamatsu Photonics, C5890-128). Nanosecond transient absorption spectra in the NIR region were measured by means of laser-flash photolysis; 532 nm light from a Nd:YAG laser was used as the exciting source, and a Ge-avalanche-photodiode module was used for detecting the monitoring light from a pulsed Xe-lamp as described in our previous report.[35−37]

Results and Discussion

The procedure developed for the triad syntheses bearing three different redox active entities, namely, ferrocene, C_{60}, and nitrobenzene/dinitrobenzene was found to be relatively simple. This involves first, the synthesis of 2-ferrocenyl fulleropyrrolidine using a procedure developed by Prato and co-workers based on 1,3-diploar cycloaddition of azomethine ylides to C_{60}.[38,39] In the second step, the secondary amino group of the pyrrolidine ring was reacted with either Sanger's reagent or dinitro/mononitro- benzoyl or benzyl chlorides followed by chromatographic purification. The ESI-mass spectra of the triads in CH_2Cl_2 matrix revealed a molecular ion peak in agreement with the calculated one. The integrated peak intensities of the ^{1}H NMR spectrum clearly established the molecular integrity of the triad. The resonance peak positions of the pyrrolidine and ferrocene entities were found at positions almost identical to that of the starting material, 2-ferrocenylfulleropyrrolidine. Only the nitroaromatic ring proton resonance peaks revealed a small shielding (0.1 to 0.2 ppm) as compared to their respective starting materials. The optical absorption spectra of the triads exhibited absorption bands corresponding to the C_{60} and nitroaromatic entities. The absorption peaks corresponding to the ferrocene entity are merged into the strong absorption bands of C_{60} and nitroaromatic entities in the 225−425 nm wavelength region for all the investigated compounds.

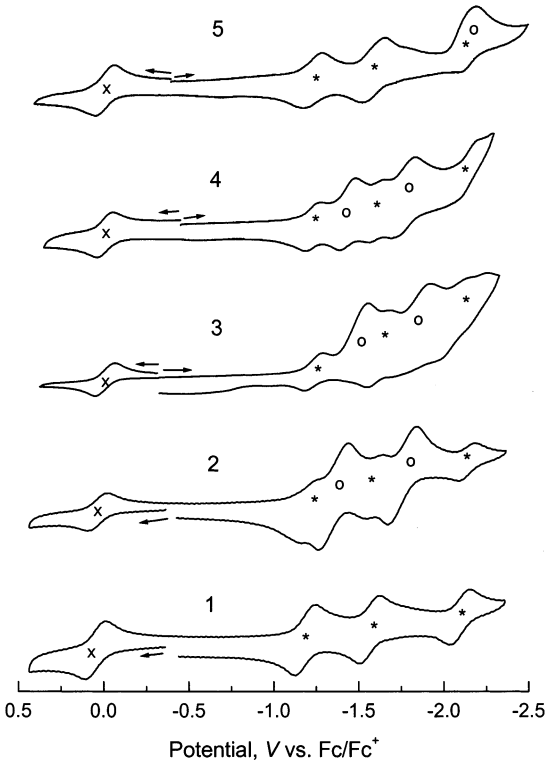

FIGURE 1. Cyclic voltammograms of investigated dyad **1** and triads **2**−**5** in 0.1 M $(TBA)ClO_4$ and *o*-dichlorobenzene. Scan rate = 0.1 V/s (x represents the Fc/Fc^+ couple, * represents the fulleropyrrolidine redox couples, and o represents redox couples corresponding to the nitroaromatic entity).

Cyclic Voltammetric Studies. Electrochemical studies using a cyclic voltammetric technique have been performed to evaluate potentials of the different redox active entities of the triad and also to visualize any electronic interactions between them. Figure 1 shows the cyclic voltammograms of the investigated compounds in *o*-dichlorobenzene containing 0.1 M $(TBA)ClO_4$, while the data are summarized in Table 1. As reported earlier,[32] dyad **1** revealed four one-electron reversible redox couples

(34) Frisch, M. J.; Trucks, G. W.; Schlegel, H. B.; Scuseria, G. E.; Robb, M. A.; Cheeseman, J. R.; Zakrzewski, V. G.; Montgomery, J. A., Jr.; Stratmann, R. E.; Burant, J. C.; Dapprich, S.; Millam, J. M.; Daniels, A. D.; Kudin, K. N.; Strain, M. C.; Farkas, O.; Tomasi, J.; Barone, V.; Cossi, M.; Cammi, R.; Mennucci, B.; Pomelli, C.; Adamo, C.; Clifford, S.; Ochterski, J.; Petersson, G. A.; Ayala, P. Y.; Cui, Q.; Morokuma, K.; Malick, D. K.; Rabuck, A. D.; Raghavachari, K.; Foresman, J. B.; Cioslowski, J.; Ortiz, J. V.; Stefanov, B. B.; Liu, G.; Liashenko, A.; Piskorz, P.; Komaromi, I.; Gomperts, R.; Martin, R. L.; Fox, D. J.; Keith, T.; Al-Laham, M. A.; Peng, C. Y.; Nanayakkara, A.; Gonzalez, C.; Challacombe, M.; Gill, P. M. W.; Johnson, B. G.; Chen, W.; Wong, M. W.; Andres, J. L.; Head-Gordon, M.; Replogle, E. S.; Pople, J. A. *Gaussian 98*, revision A.7; Gaussian, Inc.: Pittsburgh, PA, 1998.

(35) (a) Matsumoto, K.; Fujitsuka, M.; Sato, T.; Onodera, S.; Ito, O. *J. Phys. Chem. B.* **2000**, *104*, 11632−11638. (b) Komamine, S.; Fujitsuka, M.; Ito, O.; Morikawa, K.; Miyata, T.; Ohno, T. *J. Phys. Chem. A.* **2000**, *104*, 11497−11504.

(36) Nojiri, T.; Watanabe, A.; Ito, O. *J. Phys. Chem. A.* **1998**, *102*, 5215−5219.

(37) Fujitsuka, M.; Ito, O.; Yamashiro, T.; Aso, Y.; Otsubo, T. *J. Phys. Chem. A.* **2000**, *104*, 4876−4881.

(38) Maggini, M.; Scorrano, G.; Prato, M. *J. Am. Chem. Soc.* **1993**, *115*, 9798−9799.

(39) Prato, M.; Maggini, M.; Giacometti, C.; Scorrano, G.; Sandona, G.; Farnia, G. *Tetrahedron* **1996**, *52*, 5221−5234.

TABLE 1. Electrochemical Half-Wave Redox Potentials (V vs Fc/Fc^+) of the Dyad and Triads in *o*-Dichlorobenzene and 0.1 M $(TBA)ClO_4$

	potential, *E*, V vs Fc/Fc^+					
compd	$Fc^{0/+}$	$C_{60}^{0/-}$	$DNB^{0/2-}$	$C_{60}^{-/2-}$	$DNB^{2-/4-}$	$C_{60}^{2-/3-}$
1	0.06	−1.19		−1.57		−2.11
2	0.05	−1.19	−1.35	−1.58	−1.67	−2.13
3	0.02	−1.22	−1.54[a]	−1.60	−1.91[a]	−2.12
4	0.03	−1.21	−1.43	−1.58	−1.74	−2.12
5	0.03	−1.20		−1.57	−2.19[b]	−2.10

[a] $-E_{pc}$ at 0.1 V/s. [b] $-E_{pc}$ corresponding to the first reduction of the nitrobenzoyl entity.

SCHEME 2

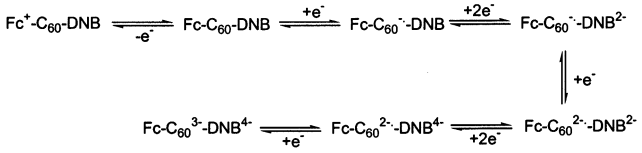

SCHEME 3

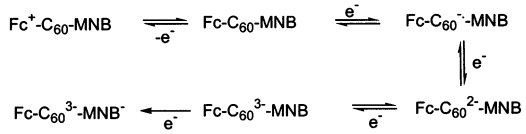

within the potential window of the solvent. It is observed that the voltammograms of the triads during the cathodic potential excursion are found to be much more complex due to the presence of the nitroaromatic entity. The redox behavior of the appended nitroaromatic entity is found to depend on the nature of the linkage to the pyrrolidine ring and the number of nitro groups. For triads **2** and **4**, bearing 3,5-dinitrobenzoyl and 3,5-dinitrobenzyl entities, respectively, two reversible redox couples are observed. It is interesting to point out that each of the reversible couples corresponds to two simultaneous one-electron transfers. The overall redox process for these two triads is summarized in Scheme 2.

For triad **3**, bearing 2,4-dinitrophenyl entity, the redox process corresponding to the reduction of this group is found to be irreversible. However, it is important to note that the cathodic peak currents are twice as large as that of the C_{60} reduction peak currents or the ferrocene oxidation peak current, indicating the occurrence of two one-electron processes for each of the redox couples. The reduction of the 4-nitrobenzoyl entity of triad **5** is found to overlap with the third reduction of the fullerene entity and is an irreversible process. This irreversibility may be due to its closeness to the potential window of the solvent. Additionally, the reduction of a 4-nitrobenzoyl group involves only a single one-electron process, which is in contradiction to the two one-electron processes observed for the dinitrobenzene bearing entities (Scheme 3). It seems that the number of nitro groups govern the total number of electrons for each of the redox processes of the nitroaromatic entity under the present solution conditions.

An examination of the data in Table 1 reveals the following, (i) The redox potentials corresponding to the ferrocene and C_{60} entities reveal small changes, suggesting little or no interactions between them or with the appended nitroaromatic entity. (ii) The potentials corresponding to the dinitrobenzene entity of triads **2**−**4** follow the order **2** < **4** < **3**, suggesting that the nature of substitution (2,4- or 3,5-) and the linking atoms to the pyrrolidine ring contribute to the overall electrochemical behavior.

Computational Studies. Prediction of accurate geometric and electronic structures of complex organic systems bearing one or more different types of redox and/or photoactive groups and subsequent reactivity of these molecular/supramolecular systems is an area of active research in computational chemistry. Although the geometric parameters can easily be predicted by semiempirical PM3 and AM1 methods, often these methods result in an incorrect electronic structure. Ab initio calculations based on either density functional theory or Hartree−Fock methods at a moderate level often yield correct geometry and electronic structure that agrees well with the experimental results. It may be mentioned here that the validity of molecular orbitals generated by density functional methods has only recently been recognized.[40] The accuracy of these methods, especially B3LYP, was recently demonstrated by Schaefer and coworkers on electron affinities of aromatic compounds[41] and by Hay on organometallic compounds.[42] In this regard, our recent study performed on **2** served as a classic example.[32] Here, the ab initio B3LYP/3-21G(*)-calculated geometry and the electronic structure followed the electrochemical observations. However, semiempirical PM3 and Hartree−Fock ab initio methods at the 3-21G(*) level resulted in either incorrect geometry or incorrect electronic structure. For this triad, PM3 calculations using *Cache MOPAC* revealed a plausible geometry but the HOMO orbitals were found to be on the C_{60} entity. The PM3 calculations performed using *SPARTAN* revealed at least three stable structures, the two low energy structures have HOMO orbitals on ferrocene, but revealed interactions between the carbonyl group or phenyl ring hydrogens of dinitrobenzoyl entity and the ferrocene iron resulting in a distorted ferrocene (the coplanarity of the two cyclopentadienyl rings was lost). The third *SPARTAN* structure was similar to the *Cache MOPAC* structure with HOMOs on the fullerene entity. Interestingly, in the structure calculated using the Hartree−Fock 3-21G(*) method optimized to a geometry close to the B3LYP structure but like the *Cache MOPAC* PM3 results, the HOMO orbitals were found to be on the fullerene entity. We did not further use these methods due to the absence of any spectroscopic evidence for such distorted geometry and electronic properties and adopted only the density functional methods.

For triad **2**, consisting of three redox active entities with little or no electronic interactions, the ab initio B3LYP/3-21G(*)-calculated results predicted the correct sequence (site) of electron transfer as revealed by the electrochemical measurements.[32] Expansion of this study involving the triads listed in Scheme 1 may serve as

(40) Stowasser, R.; Hoffmann, R. *J. Am. Chem. Soc.* **1999**, *121*, 3414−3420.
(41) (a) Brown, S. T.; Rienstra-Kiracofe, J. C.; Schaefer, H. F. *J. Phys. Chem. A* **1999**, *103*, 4065−4077. (b) Rienstra-Kiracofe, J. C.; Barden, C. J.; Brown, S. T.; Schaefer, H. F. *J. Phys. Chem. A.* **2001**, *105*, 524−528.
(42) Hay, P. J. *J. Phys. Chem. A* **2002**, *106*, 1634−1641.

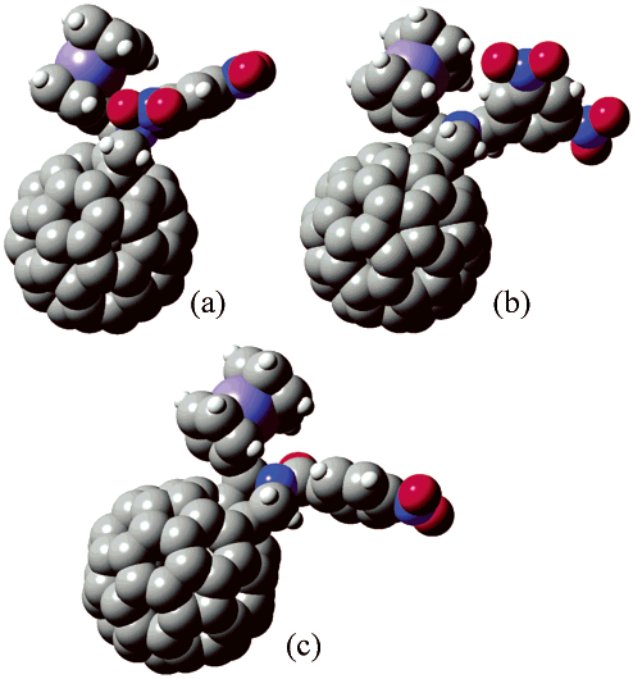

FIGURE 2. Space filling models of B3LYP/3-21G(*)-optimized structures of triads **3**−**5**.

TABLE 2. Distances between Different Redox/ Photoactive Entities of Triads Optimized by B3LYP/ 3-21G(*) Calculations

	edge-to-edge distance, Å			center-to-center distance, Å		
compd	C_{60}−Fc	C_{60}−DNB	Fc−DNB	C_{60}−Fc	C_{60}−DNB	Fc−DNB
1	2.61			8.30		
2	2.72	4.55	4.77	8.68	9.54	6.74
3	2.59	3.59	3.44	8.29	8.27	5.13
4	2.59	4.44	3.85	8.29	9.26	6.05
5	2.70	4.48[a]	4.72[a]	8.57	9.43[a]	6.81[a]

[a] Corresponds to the mononitrobenzene entity.

further confirmation about the validity of the B3LYP/3-21G(*) method for predicting the electrochemical sequence of electron transfer. Figure 2 shows the space-filling model of the energy-minimized structures on the Born−Oppenheimer potential energy surface for triads **4** and **5**, while Table 2 lists distances between the different redox/photoactive entities of the triads. In the optimized structures, the pyrrolidine ring is puckered in such a way that the 2-ferrocenyl entity is anti to the nitrogen atom and the nitroaromatic group is trans to the 2-ferrocenyl group.[43] The two cyclopentadienyl rings of the ferrocene entity form an almost eclipsed configuration. The carbon atoms of the 6,6-ring junction from which the pyrrolidine ring is formed are nearly 0.35 Å away from the positions of the normal C_{60} spheroid carbons. Earlier, an X-ray analysis of fulleropyrrolidine in a self-assembled 2-(4′-pyridyl)fulleropyrrolidine and tetraphenylporphyrinatozinc(II)[44] had revealed such structural distortions in agreement with calculations at the B3LYP/STO-3G* level. In the energy-minimized structures of the triads, this basic fullerene-ferrocene structure is retained and the nitro groups of the nitroaromatic entities are coplanar with the phenyl ring.

TABLE 3. B3LYP/3-21G(*)-Calculated Orbital Energies (in eV) for the HOMO and LUMO Orbitals of the Investigated Triads

compd	HOMO	LUMO	LUMO+1	LUMO+2	LUMO+3	LUMO+4
1	−5.57	−3.32	−3.22	−2.97		
2	−5.72	−3.60	−3.57	−3.49	−3.34	−3.24
3	−5.79	−3.63	−3.52	−3.27	−3.17	−2.88
4	−5.68	−3.54	−3.44	−3.48	−3.20	−3.18
5	−5.67	−3.54	−3.43	−3.18	−3.09	

The edge-to-edge and center-to-center distances between the different redox/photoactive entities of the dyad and triads are summarized in Table 2. For estimation of the edge-to-edge distances, the closest carbon atom of one entity to the closest atom of the neighboring entity was considered. For the estimation of the center-to-center distances, the center of C_{60}, the position of iron in ferrocene, and the center of the phenyl ring of the nitroaromatic entities were considered. An examination of the data given in Table 2 reveals the following. (i) The edge-to-edge distances and center-to-center distances between the C_{60}−Fc entities are the shortest ones followed by the distances bewteen Fc−DNB and C_{60}−DNB. (ii) Among the different triads, compound **3** has the shortest Fc−DNB and C_{60}−DNB intergroup distances due to the direct connection between the DNB to the pyrrolidine ring. The intergroup distances between the different entities are important since the rates of photoinduced electron transfer are expected to show a distance dependency. As discussed later in this manuscript, this is indeed true for the investigated series of triads.

The sequence of the site of electron transfer during electrochemical measurements in these triads is modeled by observing the frontier HOMO and LUMO molecular orbitals. Figures 3 and 4 shows the first HOMO and the first five LUMO orbitals of triads **4** and **5**, and Table 3 summarizes the energies of these orbitals for all the investigated triads, including dyad **1**. For all the investigated compounds, in agreement with the electrochemical results, the frontier HOMO is found to be located on the ferrocene entity (Figures 3a and 4a). Interestingly, as expected from the electrochemical data, the majority of the frontier LUMO is located on the C_{60} spheroid for all the derivatives (Figures 3b and 4b). The calculated (gas phase) HOMO−LUMO gap is found to range between 2.12 and 2.25 eV and compares with the electrochemically measured (difference between the first oxidation and first reduction potential) values ranging between 1.23 and 1.25 V. Apparently, the magnitude of the HOMO−LUMO gap remains almost the same for the dyad and the triads, a trend that is consistent with the electrochemical observations. The orbital energies of the subsequent LUMO orbitals are found to vary a little depending up on the nature of the nitroaromatic entity of the triads although a specific trend is difficult to discern.

The coefficients of the subsequent LUMO orbitals are shown in Figures 3 and 4. The location of the coefficients of the HOMO and LUMO orbitals for triads **2**−**4** follows the order: C_{60}, dinitrobenzene, C_{60}, dinitrobenzene, and C_{60} entities, a trend that tracks exactly the sequence (site)

(43) D'Souza, F.; Zandler, M. E.; Deviprasad, G. R.; Kutner, W. *J. Phys. Chem. A.* **2000**, *104*, 6887−6893.
(44) D'Souza, F.; Rath, N. P.; Deviprasad, G. R.; Zandler, M. E. *Chem. Commun.* **2001**, 267−268.

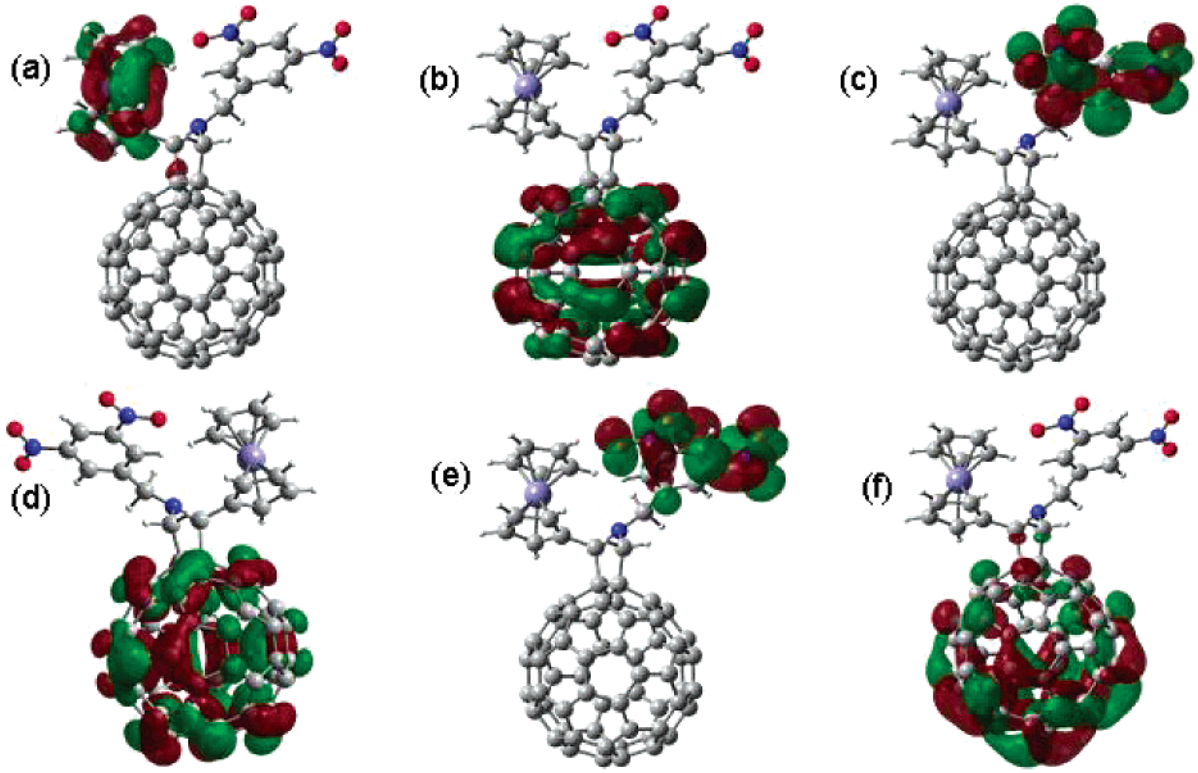

FIGURE 3. Ab initio B3LYP/3-21G(*)-calculated frontier (a) HOMO, (b) LUMO, (c) LUMO + 1, (d) LUMO + 2, (e) LUMO + 3, and (f) LUMO + 4 orbitals of triad **4**.

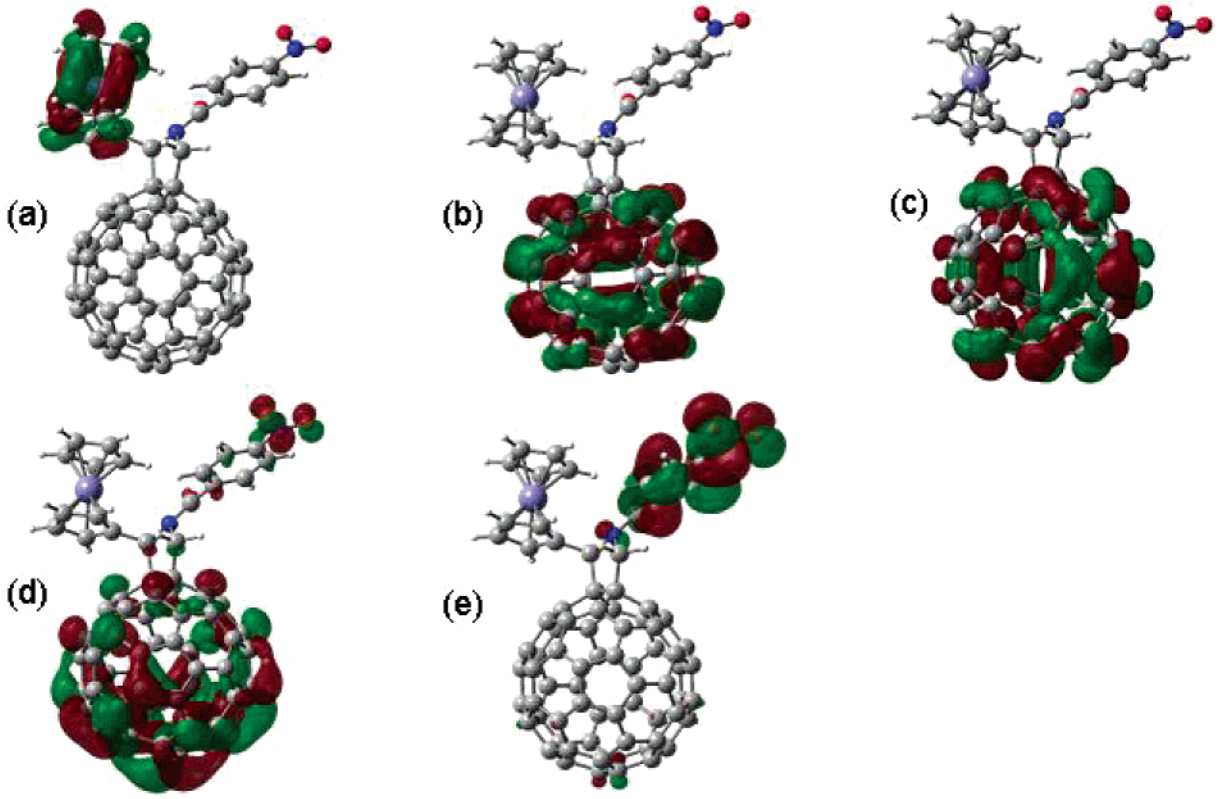

FIGURE 4. Ab initio B3LYP/3-21G(*)-calculated frontier (a) HOMO, (b) LUMO, (c) LUMO + 1, (d) LUMO + 2, and (e) LUMO + 3 orbitals of triad **5**.

of electron transfer of the triad as depicted in Scheme 2. Interestingly, for triad **5**, in which the nitrobenzoyl reduction overlaps with the third reduction of the C_{60} entity, the frontier HOMO and LUMO orbitals are shown

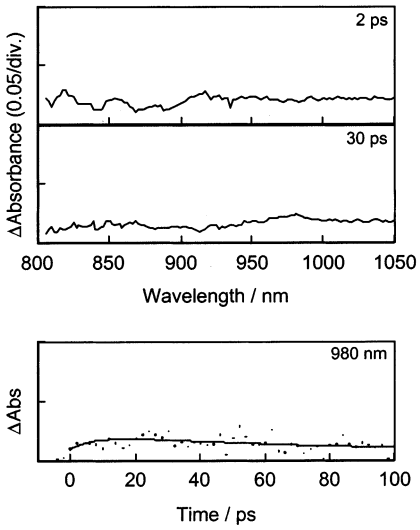

FIGURE 5. (Upper panel) Transient absorption spectra of **3** in benzonitrile at 2 and 30 ps after laser irradiation (388 nm, <150 fs). (Lower panel) Absorption time profiles at 980 nm for **3**. Solid lines are fitted curves assuming rise and decay of 1.5×10^{11} and 7.0×10^{9} s^{-1} of rate constants, respectively.

in Figure 4. The sequence of molecular orbital coefficients involving the first HOMO and four LUMO orbitals follows the order: ferrocene, C_{60}, C_{60}, C_{60} and nitrobenzene, a trend that agrees readily with the electrochemical results summarized in Scheme 3. Note the delocalization of orbital regions over the C_{60} and nitrobenzoyl entities in the LUMO + 2 corresponding to the electrochemical reduction potential overlap.

The general agreement between electrochemical site of electron transfer and computational results of the present are commendable, suggesting that the B3LYP/3-21G(*) methods could be more suitable for modeling the electronic structures of similar or more complex molecular/supramolecular systems. However, the computed gas-phase HOMO−LUMO gaps are nearly 1 eV higher than those measured by electrochemical methods, and this trend is consistent for all of the studied compounds.

Photochemical Studies. The room-temperature fluorescence emission intensity of the triads in benzonitrile, excited at 390 nm and monitored in the wavelength region of fulleropyrrolidine emission[32,33c] (650−750 nm), was found to be totally quenched for all the investigated triads. This indicates the occurrence of excited-state processes from the singlet excited fulleropyrrolidine. To verify the quenching mechanism and characterize the reaction products, subpicosecond as well as nanosecond transient absorption studies on both the dyad and triad have been performed.

Transient spectral results for triad **3** observed after the 150 fs laser excitation at 388 nm in benzonitrile are shown in Figure 5. Immediately after the laser pulse, a broad transient absorption band appeared at 3 ps in the wavelength region from 800 to 1050 nm, and this has been attributed to the singlet−singlet absorption of the fulleropyrrolidine entity.[36] For triads **4** and **5**, similar transient spectra were observed. At 30 ps, a sharp band at 980 nm corresponding to the radical anion of the fulleropyrrolidine entity[37] was also observed. From the rise of this band, the evaluated rate of charge separation (k_{CS}) generating the ion-pair state was found to be 1.5×10^{11} s^{-1} and the decay rate of the ion-pair state (k_{CR}) was evaluated to be 7.0×10^{9} s^{-1}. For triad **5**, the rate of the k_{CS} was found to be 1.1×10^{11} s^{-1} and the k_{CR} was evaluated to be 1.3×10^{9} s^{-1}. In the case of triad **4**, the rate constants were not evaluated, because of their noisy time profiles. The larger k_{CS} value reported earlier for triad **2**[32] compared to those for **3** and **5** may be attributed to the electron-withdrawing >C═O group (Table 4). The larger k_{CR} for triad **3** compared to that for **2** may be attributed to the smaller intermoiety distances for **3** (Table 2) as a result of the direct connection of the dinitrobenzene group to the pyrrolidine ring. The smaller k_{CR} for triad **5** compared to that for **3** may be due to the weaker electron acceptor ability of the mononitrobenzene moiety.

TABLE 4. Rate Constants for Charge Sepration (k_{CS}) and Charge Recombination (k_{CR}) in *o*-Dichlorobenzene for the Investigated Dyad and Triads

compd	k_{CS}/s^{-1}	k_{CR}/s^{-1}
1	2.5×10^{11} [a]	8.5×10^{9} [a]
2	2.2×10^{11} [a]	4.5×10^{9} [a]
3	1.5×10^{11}	7.0×10^{9}
4		
5	1.1×10^{11}	1.3×10^{9}

[a] From ref 32.

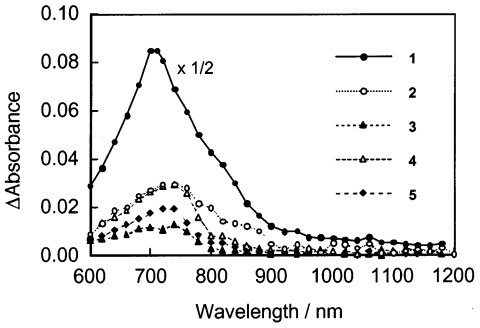

FIGURE 6. Transient absorption spectra of (a) 2-phenyl fulleropyrrolidine, (b) **1**, (c) **2** (d) **3**, (e) **4**, and (f) **5** in benzonitrile at 100 ns after laser irradiation (352 nm, 6 ns).

Figure 6 shows the transient absorption spectra observed after nanosecond laser excitation of compounds **1**−**5**. As reported in our previous paper,[32] 2-phenyl fulleropyrrolidine bearing no redox active entities showed an additional intense transient band at 720 nm with a shoulder at 850 nm, which was attributed to the triplet−triplet absorption, generated via the intersystem crossing from the singlet excited state within 1.2 ns; the intensity of the absorption maximum decays slowly with a rate constant of 1.6×10^{5} s^{-1}. In the case of dyad **1** (Figure 6), the shape of the absorption band is similar to that of fulleropyrrolidine, indicating the formation of the triplet state of the fullerene entity, which is also supported by a similar decay rate constant of 2.5×10^{5} s^{-1}. However, the absorption intensity is low by a factor of about 1/8, suggesting that most of the excited singlet state undergoes the charge separation process rather than formation of a C_{60} triplet state directly.

The absorption intensity of the transient absorption band of **2** is found to be considerably lower than that of

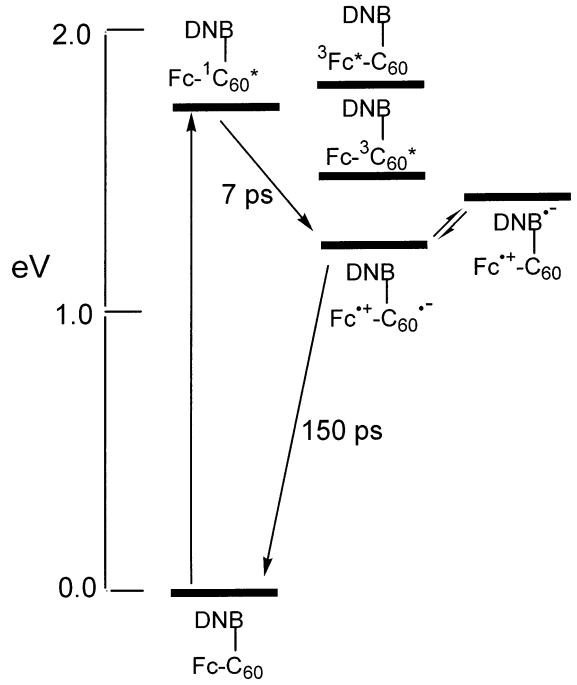

FIGURE 7. Energy level diagram depicting photoinduced events for the fullerene−ferrocene−dinitrobenzene bearing triads in benzonitrile.

1 (about 1/6). Although the peak at 720 nm is broad, this weak absorption has also been attributed to the triplet state since the lifetime is almost the same as that obtained for fulleropyrrolidine (rate constant = 1.9×10^5 s^{-1}). One of the reasons for the low distribution of the triplet states of **1** and **2** may be the charge separation process of **1** and **2** via their singlet excited states. Almost similar behavior is observed for the investigated triads **3**−**5**. It may also be noted that the intensity of the transient absorption band of **3** is smaller than that of both triad **2** and **4**, and this has been attributed to the close proximity (no connecting atoms) of the dinitrobenzene entity to the fulleropyrrolidine group in **3**. The higher intensity of **5** compared to that of **3** suggests that the electron acceptor ability of the dinitrobenzene moiety is stronger than that of the mononitrobenzene moiety (Table 1). The measured decay rate constants of the triplet states were found to be ca. 2×10^6 s^{-1} for **3**−**5**.

Figure 7 illustrates the energy level diagram for the different photochemical events of triads **2**−**5**. The lower triplet yields of **2**−**5** compared to that of fulleropyrrolidine, which has the high quantum yield of intersystem crossing of the singlet excited state,[32] suggest that the triplet state of **2**−**5** is at a higher energy level than that of the ion-par state and that the triplet states are partially formed via the charge recombination. The observed fast charge separation rates in the triads are in good agreement with lower ion-pair states compared with the triplet states. That is, the energy gaps between the singlet excited states and the ion pair states are about 0.5 eV, which may be almost the top region of the Marcus parabola for fullerene derivatives.[45] This suggests the unlikely formation of a direct triplet state of the fullerene entity via intersystem crossing of the singlet excited state, which is in good agreement with the observed decrease in the formation of the triplet excited state in Figure 6. The relatively faster charge recombination rates of the ion-pairs of triads **2**−**5** could be attributed to spatial back electron transfer from the dinitrobenzene entity to the ferrocene entity. This provides indirect evidence for the migration of the electron toward the dinitrobenzene entity in the ion pair states of triads **2** and **3**, although this process is energetically unfavorable. This unique photochemical and photophysical behavior is further supported by the ab initio-calculated distribution of LUMO orbital coefficients.

Summary. Synthesis of a series of triads composed of three redox active entities, namely, ferrocene, C_{60}, and nitroaromatic entities, has been accomplished. Electrochemical studies revealed multiple redox processes involving all three redox active entities. Computational calculations performed using ab initio B3LYP/3-21G(*) methods predicted a plausible geometry and electronic structure of the investigated triads. The HOMO orbital calculated by the B3LYP/3-21G(*) method was found to lie primarily on the ferrocene entity, while the LUMO orbitals are located on the C_{60} entity except for the case of **2**, where small orbital coefficients are also found on the dinitrobenzene entity. The orbital coefficients of the subsequent LUMO orbitals track the observed site of electrochemical reductions of the triads, suggesting that B3LYP/3-21G(*) methods could be more suitable for modeling the geometric and electronic structures of complex molecular systems. Time-resolved picosecond transient absorption studies revealed efficient charge separation and charge recombination in the studied triads, and this has been attributed to the close spacing of the entities of the triad relative to one another.

Acknowledgment. The authors are thankful to the donors of the Petroleum Research Fund, administered by the American Chemical Society, and National Institutes of Health for support of this work. P.M.S. is thankful to the Department of Education for a GAANN fellowship. The authors are also thankful to the High Performance Computing Center of the Wichita State University for lending SGI ORIGIN 2000 computer time. O.I. and M.F. are thankful to the Mitsubishi Foundation and the Ministry of Education, Science Technology, Culture, and Sports of Japan.

Supporting Information Available: ^{1}H NMR spectra of compounds **3**−**5**, B3LYP/3-21G(*)-computed Cartesian coordinates, and the total energy of the investigated compounds **1**−**5**. This material is available free of charge via the Internet at http://pubs.acs.org.

JO020417I

(45) Imahori, H.; Tamaki, K.; Gulidi, D. M.; Luo, C.; Fujitsuka, M.; Ito, O.; Sakata, Y.; Fukuzumi, S. *J. Am. Chem. Soc.* **2001**, *123*, 2607−2617.